Journal of Hydrology 554 (2017) 600–612

Contents lists available at ScienceDirect

Journal of Hydrology

journal homepage: www.elsevier.com/locate/jhydrol

Research papers

Hydraulic-based empirical model for sediment and soil organic carbon loss on steep slopes for extreme rainstorms on the Chinese loess Plateau

L. Liu [a,e], Z.W. Li [a,b,*], X.D. Nie [a,b], J.J. He [c,*], B. Huang [d], X.F. Chang [a], C. Liu [a,b], H.B. Xiao [a], D.Y. Wang [b]

[a] State Key Laboratory of Soil Erosion and Dryland Farming on the Loess Plateau, Institute of Soil and Water Conservation, CAS and MWR, Yangling, Shaanxi Province 712100, PR China
[b] College of Environmental Science and Engineering, Hunan University, Changsha 410082, PR China
[c] Base of the State Laboratory of Urban Environmental Processes and Digital Modeling, Key Laboratory of 3D Information Acquisition and Application, Ministry of Education, Capital Normal University, Beijing 100048, PR China
[d] Guangdong Key Laboratory of Agricultural Environmental Pollution Integrated Control, Guangdong Institute of Eco-environment Technology, Guangzhou 510650, PR China
[e] Graduate University of Chinese Academy of Sciences, Beijing 100049, PR China

ARTICLE INFO

Article history:
Received 6 May 2017
Received in revised form 2 September 2017
Accepted 4 September 2017
Available online 22 September 2017
This manuscript was handled by G. Syme, Editor-in-Chief

Keywords:
SOC loss
Soil erosion
Simulated rainfall
Hydraulic factor
Model

ABSTRACT

Building a hydraulic-based empirical model for sediment and soil organic carbon (SOC) loss is significant because of the complex erosion process that includes gravitational erosion, ephemeral gully, and gully erosion for loess soils. To address this issue, a simulation of rainfall experiments was conducted in a 1 m × 5 m box on slope gradients of 15°, 20°, and 25° for four typical loess soils with different textures, namely, Ansai, Changwu, Suide, and Yangling. The simulated rainfall of 120 mm h^{-1} lasted for 45 min. Among the five hydraulic factors (i.e., flow velocity, runoff depth, shear stress, stream power, and unit stream power), flow velocity and stream power showed close relationships with SOC concentration, especially the average flow velocity at 2 m from the outlet where the runoff attained the maximum sediment load. Flow velocity controlled SOC enrichment by affecting the suspension–saltation transport associated with the clay and silt contents in sediments. In consideration of runoff rate, average flow velocity at 2 m location from the outlet, and slope steepness as input variables, a hydraulic-based sediment and SOC loss model was built on the basis of the relationships of hydraulic factors to sediment and SOC loss. Nonlinear regression models were built to calculate the parameters of the model. The difference between the effective and dispersed median diameter (δD_{50}) or the SOC content of the original soil served as the independent variable. The hydraulic-based sediment and SOC loss model exhibited good performance for the Suide and Changwu soils, that is, these soils contained lower amounts of aggregates than those of Ansai and Yangling soils. The hydraulic-based empirical model for sediment and SOC loss can serve as an important reference for physical-based sediment models and can bring new insights into SOC loss prediction when serious erosion occurs on steep slopes.

1. Introduction

Soil erosion can remove a significant portion of soil organic matter (SOM) (Lal, 2005; Schiettecatte et al., 2008a); such process is important to agricultural productivity (Prokop and Poręba, 2012; Yitbarek et al., 2012) and sustainable resource management (Li et al., 2017; Zhao et al., 2013). Meanwhile, soil organic carbon (SOC) mobilized by erosion can be lost to the atmosphere within a short period or transported off site (Polyakov and Lal, 2008). Breakup of initial soil aggregates by erosive forces increases CO_2 emission. Breakdown of aggregates causes exposure of encapsulated C to microbial processes, thereby increasing SOC mineralization rate (Lal, 2003). Thus, SOC loss accompanied with soil erosion is an important component of the net ecosystem carbon balance (Nadeu et al., 2014; Wang et al., 2014). However, in recent years, researchers have focused mainly on the SOC stability (Berhe and Kleber, 2013), SOC mineralization (Gregorich et al., 2015), SOC stocks (Li et al., 2017), or redistribution of SOC after erosion (Liu et al., 2017). SOC loss is mainly understood by sediment erosion (Palis et al., 1997). Although hydraulic process controlling sediment loss has been widely studied (Pan and Shangguan, 2006; Slattery and Bryan, 1992), the direct relationships between hydraulic factors and SOC concentration are yet to be studied for any soil in building a hydraulic-based SOC loss model.

* Corresponding authors at: State Key Laboratory of Soil Erosion and Dryland Farming on the Loess Plateau, Institute of Soil and Water Conservation, CAS and MWR, Yangling, Shaanxi Province 712100, PR China (Z.W. Li).
E-mail addresses: lizw@hnu.edu.cn (Z.W. Li), Hejiun_200018@163.com (J.J. He).

https://doi.org/10.1016/j.jhydrol.2017.09.010
0022-1694/

SOC loss is usually estimated by sediment loss (Häring et al., 2014; Li et al., 2016c). A few physical-process sediment models, such as Water Erosion Prediction Project (WEPP), have been built (Foster et al., 1995; Nearing et al., 1989). However, WEPP, which is a widely used physical-based model, is a steady state model and cannot obtain high-sediment prediction accuracy when complex erosion processes occur, such as gravitational erosion, ephemeral gully, and gully erosion (Zheng, 2006). In China, serious erosion usually occurs on farmlands with steep slopes (Fu, 1989); this serious erosion is usually accompanied with gravitational erosion, ephemeral gully, and gully erosion on the hill slopes on the Loess Plateau (Zheng, 2006). Therefore, building a hydraulic-based sediment and SOC loss model can provide a reference for the SOC loss prediction and help improve WEPP applicability in China. Sediment transport capacity is usually calculated by runoff rate, slope, and flow velocity (Govers, 1990; Quinton et al., 2006; Schiettecatte et al., 2008b), and flow velocity is a good predictor of sediment concentration (Arjmand and Mahmoodabadi, 2015). A hydraulic-based sediment and SOC loss model can be built by clarifying the relationship between hydraulic factors and SOC concentration.

In recent decades, SOM dynamic models, such as Century (Smith et al., 1997) or erosion productivity impact calculator models (Sharpely and Williams, 1990) mainly focusing on the SOC change of the ecosystem, have been proposed. SOC loss is an important component of SOC dynamic models and is calculated mainly by two methods (Häring et al., 2014; Li et al., 2016c). In the first traditional method, cumulative SOC loss is simply calculated as the product of SOC concentration, SOC enrichment ratio, and cumulative sediment loss. According to our previous study (Li et al., 2016c), the predicted precision of traditional method is low under high rainfall intensity for loess soils. The second method is the recently developed carbon, input, decomposition, and erosion (CIDE) approach. CIDE calculates SOC loss on the basis of the comparison between un-eroded and eroded cultivated sites; this method requires large amounts of costly input variables (e.g., carbon isotope) (Häring et al., 2013). Therefore, building a hydraulic-based SOC loss model, which is rational and scientific, may be significant for SOC prediction when severe erosion occurs.

On average within 100 years, 50% of SOM transported off site can be attributed to erosion on steep slopes (Polyakov and Lal, 2004). Soil texture demonstrates a major control over organic matter dynamics, and clay percentage determines the SOC concentration of sediments (Avnimelech and McHenry, 1984; Parton et al., 1987). Therefore, steep slope and soil texture were the two main factors considered in our study. The present study aimed to (i) investigate the effect of hydraulic factors on sediment SOC concentration for four loess soils with different soil textures on steep slopes and (ii) build a hydraulic-based sediment and SOC loss model for providing options and references for soil loss and SOC dynamic models.

2. Methods and materials

2.1. Experimental devices

Simulated rainfall experiments were conducted at the State Key Laboratory of Soil Erosion and Dryland Farming on the Loess Plateau. A down sprinkler rainfall simulator device with a rainfall intensity ranging from 30 mm h^{-1} to 350 mm h^{-1} was used to simulate rainfall; rainfall intensity was also adjusted by the change in nozzle size and water pressure (Shen et al., 2016). Prior to performing the experiments, rainfall intensity calibration was conducted to reach the target of rainfall intensity with a uniformity of > 0.90. The structure of the soil pan constructed with metal sheets was 5 m (length) × 1 m (width) × 0.5 m (depth); a metal runoff collector was set at the end of the soil pan (Shi et al., 2012). The slope of the pan could be electronically adjusted to a desired slope between 0° and 30°. Tap water (electrical conductivity = 0.7 dS m^{-1}) was used for all experiments. The soils used in the experiments were four loess soils with clay contents of 26%, 21%, 16%, and 12%. The sample sites were Suide (37 °29′N, 110 °14′E), Changwu (35 °22′N, 107 °80′E), Yangling (34 °16′N, 108 °4′E), and Ansai (36 °58′N, 109 °20′E); these sites are distributed from south to north across the Loess Plateau of China (Fig. S1). The four sampled fields have been cultivated with crops for many years. Thus, the sampling depth was 20 cm. Sampling time was before the crop cultivation. The properties of the loess soils are shown in Table 1. The basic properties of soil were determined using standard analytical methods (Finkner and Gilley, 1988).

2.2. Rainfall simulation experiments

All soil samples were air dried to ~10% moisture content (gravimetric) and were passed through a 10 mm sieve. The soil pan was packed with the bulk density, as presented in Table 1. Before packing the plow layer, a 10 cm-thick layer of coarse sand was added to the bottom of the experiment plot to maintain permeable conditions. Subsequently, fine gauze was placed on top of the layer of coarse sand. Finally, a 30 cm-thick soil layer was laid on the coarse sand layer at 5 cm increments. Each layer of the plot was raked lightly to ensure uniformity and continuity in soil structure. The packed soil samples were ensured to be coherent with the wall by gluing the soil into the tray wall to avoid ponding water. Considering the similarity of soil properties at different slope locations (e.g., slope positions or slope angles) for each soil, three typical slope gradients of 15°, 20°, and 25° were applied. The slope gradient of 25° corresponded with the maximum slope for cultivated land according to the classification of farmland slopes in the Loess Plateau (Comprehensive Scientific Expedition, 1990). Prior to simulating rainfall, the plot slope was adjusted to a desired slope. The soil samples were wetted from the top with water applied as mist. After the soils reached full saturation, the plots were exposed to a simulated rainfall of 120 mm h^{-1}, a peak intensity of strong storms in the subhumid climatic regions of China (Cai et al., 1998; Chen, 1987). A total of 12 treatments were conducted (4 × soils with 3 × slope angles each). Each treatment was repeated by repacking the plot and repeating the simulated rainfall process and was tested in two replicates. The experimental results of the repeated treatments did not show a significant difference and were consistent with that in the experiment conducted by Wang and Shi (2015), who focused on the size selective erosion of the same two loess soils.

2.3. Measurements

2.3.1. Sediment and SOC measurements

For each rainfall event, runoff was volumetrically measured and sampled at 1 min intervals for sediment concentration after initiation. Each sample was dried and weighed in forced-air ovens at 60 °C for 24 h. During the rainfall, the runoff-yield time, rill initiation times, rill location, and rill shape were also recorded. The rill width, length, and location were frequently measured with a millimeter-scale ruler at numerous locations. Sediment transport and soil surface conditions were visually observed and recorded during and after simulating storms. Sediment concentration was determined by the ratio of each dry sediment mass to sampled runoff volume. Meanwhile, total sediment loss was defined as the total sediment load present in runoff water. The SOC concentration of each sample was determined using the dichromate oxidation method (Walkley and Black, 1934) and was defined as the

Table 1
Properties of selected soils from Suide, Ansai, Yangling, and Changwu (Means ± RMSE).

Property	Clay (%)[a]	Fine silt[a] (%)	Coarse silt[a] (%)	Fine sand[a] (%)	Coarse sand[a] (%)	$CaCO_3$ (g kg^{-1})	Bulk density (g cm^{-3})	PH	Soil organic carbon (SOC) (g kg^{-1})
Suide	12.1 ± 1.7	19.4 ± 1.0	36.3 ± 1.5	26.5 ± 2.1	5.6 ± 1.5	115.2 ± 2.3	1.25	8.6 ± 0.2	2.06 ± 0.1
Ansai	15.6 ± 1.5	26.8 ± 1.0	38.1 ± 0.7	14.6 ± 1.1	4.8 ± 1.2	103.7 ± 3.1	1.20	8.4 ± 0.2	4.62 ± 0.2
Yangling	26.3 ± 2.9	38.1 ± 0.5	28.7 ± 1.0	5.6 ± 0.6	1.3 ± 0. 6	75.4 ± 1.8	1.30	8.3 ± 0.3	5.68 ± 0.2
Changwu	21.2 ± 3.6	38 ± 1.0	31.3 ± 0.9	5.6 ± 2.0	3.9 ± 1.7	81.1 ± 5.6	1.20	8.3 ± 0.2	6.36 ± 0.3

[a] Soil texture is classified on the basis of the USDA soil classification system.

SOC load per kilogram of sampled sediments. SOC loss was defined as the total SOC load present in sediment loss.

2.3.2. Determination of hydraulic parameters and flow characteristics

A fluorescent dye was used for flow velocity measurement (Gilley et al., 1990). A dye tracer was used, and its travel time from the injection point to a downslope point was measured visually. Surface velocity of overland flow was obtained by dividing travel distance by travel time. Meanwhile, flow velocity was measured across a distance of 50 cm successively at four locations within the plot as follows: 75–125, 175–225, 275–325, and 375–425 cm from the outlet. These values were referred to as 1, 2, 3, and 4 m locations, respectively. The flow velocity at the 1 m location was measured initially. Then, the flow velocity of 2 m location was measured, and so on, for each of the four locations. After measuring the velocity at the 4 m location, the flow velocity at 1 m location was measured again. The measurement was completed by one person for one of the two replicated plots to reduce experimental error. A correction factor α was also applied to convert the surface velocity of the flow to average velocity (Zhang et al., 2010). The correction factor increased with velocity or with Reynolds number for laminar flow and could be as high as 0.83 for turbulent flow (Planchon et al., 2005). The correction factor α of sediment-laden flow varied from 0.233 to 0.682 with a mean value of 0.466. Thus, we selected 0.466 as the correction factor for interrill flow and 0.8 as the correction factor for rill flow (Wang and Shi, 2015). During rainfall, the rill erosion was observed at the measured location. Thus, the flow velocity after the time of rill initiation belonged to the flow velocity of rill flow. The runoff depth, shear stress, stream power, and unit stream power were determined as follows (Mahmoodabadi et al., 2014; Nearing et al., 1997):

$$D = \frac{q}{V}, \tag{1}$$

$$\tau = \rho g D S, \tag{2}$$

$$\omega = \rho g S q, \tag{3}$$

$$\Omega = V S, \tag{4}$$

where D is the average flow depth (m), q is the average unit flow discharge per unit width ($m^2\ s^{-1}$), V is the measured flow velocity ($m\ s^{-1}$), τ is the shear stress (Pa), ρ is the density of water (g cm^{-3}), g is the gravitational constant (cm s^{-2}), S is the slope gradient ($m\ m^{-1}$), ω is the stream power (g s^{-3}), and Ω is the unit stream power ($m\ s^{-1}$).

2.3.3. Measurements of sediment particle size distribution

The samples for the sediment particle size distribution analysis were first analyzed with a Malvern Mastersizer 2000 laser diffraction device (Malvern Instruments Ltd., UK) without a dispersion treatment to obtain the undispersed sediment particle size distribution and the median diameter of each sample. Thereafter, the samples were treated with H_2O_2 to remove organic matter and with sodium hexametaphosphate for chemical dispersion before being subjected to ultrasonic dispersion. Then, the particle size distribution of dispersed sediment and the median diameters of each sample were analyzed with the laser diffraction device. The median diameter difference of effective to dispersing sediment particles (δD_{50}) was calculated by the equation as follows:

$$\delta D_{50} = D_{e,50} - D_{d,50}, \tag{5}$$

where $D_{e,50}$ is the median particle size of the undispersed soil and $D_{d,50}$ is the median particle size of the dispersed soil.

2.4. Sediment and SOC loss model

In process-based sediment models, such as WEPP, sediment loss is mainly related to the transport capacity (Tc), which is generally estimated by hydraulic parameters, sediment particle size distribution, and slope (McHugh et al., 2002; Nearing et al., 1989). A widely applied Tc equation, which is used in Limburg Soil Erosion Model (LISEM) (De Roo et al., 1996) and European Soil Erosion Model (EUROSEM) (Morgan et al., 1998), was proposed by Govers (1990). The transport capacity equations proposed by Govers (1990) could be predicted by unit stream power, Ω ($m\ s^{-1}$), as follows:

$$Q_S = \rho_S Q a [100(\Omega - \Omega_{cr})]^b, \tag{6}$$

$$a = \left[\frac{D_{50} + 5}{0.32}\right]^{-0.6}, \tag{7}$$

$$b = \left[\frac{D_{50} + 5}{300}\right]^{0.25}, \tag{8}$$

where Q_s is the total sediment discharge ($kg\ s^{-1}$); ρ_s is the material density ($kg\ m^{-3}$); Q is the total runoff discharge ($m^3\ s^{-1}$); Ω_{cr} is the critical unit stream power (0.004 $m\ s^{-1}$ for a wide range of materials); a and b are regression coefficients related to the median particle diameter, D_{50} (μm). Slope and flow velocity exhibited the same contribution for this transport capacity estimation because unit stream power was the product of slope and flow velocity. However, slope and flow velocity showed different contributions to sediment loss (Hessel and Jetten, 2007; Mahmoodabadi et al., 2014). Therefore, sediment loss was directly predicted by flow velocity, slope, and other affecting factors that might be effective. By revising the transport capacity equations proposed by Govers (1990), sediment loss was calculated by the equation as follows:

$$E_s = 1000 \times a \times \rho_s \times q_s \times t \times V_s^b \times S^c, \tag{9}$$

$$a = y0 - Ae^{km}, \tag{10}$$

$$b = yo + A\ln(km), \tag{11}$$

$$c = y0 + Ae^{kC_{soc}}, \tag{12}$$

where E_s is the total sediment loss (kg); q_s is the runoff rate ($ml\ s^{-1}$); t is the runoff time (s); V_s is the average flow velocity at the location where runoff becomes transport limited ($m\ s^{-1}$); C_{soc}

is the SOC content in the original soils; m is the δD_{50} (μm) of original soil; a, b, c, $y0$, A, and k are the regression coefficients.

On the basis of the mechanism of flow velocity controlling SOC concentration and relationship of SOC loss and stream power investigated in our study, the SOC loss mass at the foot of hill slope was calculated by the following equation:

$$C_{Loss} = 1000 \times a_{\times} \rho_s \times C_{SOC} \times q_s \times t \times V_s^b \times S^c, \quad (13)$$

where C_{Loss} is the total SOC loss (g), and C_{soc} is the SOC content in the original soils (g kg^{-1}). The regression coefficients a, b, and c could also be calculated using Eqs. (10)–(12).

2.5. Data treatment

All statistical analyses, except principal component analysis (PCA) and correlation analysis, were performed using SPSS 19.0. All graphics, except the biplot, were drawn using Origin 8.0 software. PCA and correlation analysis were conducted using SAS JMP 11.0. PCA analyzes several dependent variables, which are generally intercorrelated, and extracts and expresses the important information from variables using a set of new orthogonal variables called principal components (PCs, Abdi and Williams, 2010; Meyers et al., 2006). PC is obtained as linear combinations of the original variables. The Kaiser–Meyer–Olkin (KMO) measure of sampling adequacy is a statistic that indicates the proportion of variance in variables that may be caused by underlying factors. Values greater than 0.50 generally indicate that PCA is useful for the data because the patterns of correlations are relatively compact. Bartlett's test of sphericity tests the hypothesis that the correlation matrix is an identity matrix, which indicates that the variables are unrelated and therefore unsuitable for structure detection (Armentano et al., 2015). From our data, the KMO was 0.655, and the Bartlett test was significant ($P < 0.01$). Thus, the data of the following 11 parameters were all incorporated into the PCA: sediment concentration, total sediment loss, SOC concentration, total SOC loss, effective median diameter of sediments, median diameter difference between the effective and dispersed sediments, flow velocity at locations 1, 2, 3, and 4 m, and SOC enrichment. Prior to the PCA analysis, the data table was standardized. A scatter plot map of the variables (i.e., average flow velocity at four locations and percentage of different sediment particle size) and a three-dimensional (3 D) "point cloud" fitted by ellipsoid, which were built to detect the interaction effect of factors (e.g., flow velocity and δD_{50}) on sediment loss, were obtained by correlation analysis. Average flow velocities were used in our analysis for each treatment. A one-way analysis of variance [Duncan's test ($\alpha = 0.05$)] was used to compare the SOC concentration, sediment concentration, total sediment loss, or total SOC loss for different treatments. Three statistical procedures were used to assess the agreement between the predicted and observed data as follows:

1) The average error produced by a model is encapsulated in the root mean squared error (RMSE), which is frequently used to evaluate models and shown as follows:

$$RMSE = \sqrt{\sum_{i=1}^{n} \frac{(P_i - Q_i)^2}{n}}, \quad (14)$$

2) The efficiency of a model is defined by R^2 (analogous to the coefficient of determination) as the proportion of the initial variance accounted for by that model (Nash and Sutcliffe, 1970) and calculated as follows:

$$R^2 = 1 - \frac{\sum_{i=1}^{n} (P_i - O_i)^2}{\sum_{i=1}^{n} (O_i - O)^2}, \quad (15)$$

3) This new descriptive statistic (d) reflects the degree to which the observed variate is accurately estimated by the simulated variate, thereby representing the ratio of the mean square error and the potential error (Willmott, 1981), as follows:

$$d = 1 - \frac{\sum_{i=1}^{n} (P_i - O_i)^2}{\sum_{i=1}^{n} (|P_i - O| + |O_i - O|)^2}, \quad (16)$$

where n is the number of samples; P_i and O_i are the predicted and observed values, respectively. O is the mean of the observed data. An RMSE value close to 0 means the model is accurate. The modeling efficiency (R^2) and agreement index (d) represent a perfect match between modeled values and observed data when the values of R^2 and d are close to 1.

3. Results

3.1. Features of sediment and SOC loss

Fig. 1 shows that, under the high-rainfall intensity of 120 mm h^{-1} on the Loess Plateau, the SOC loss did not always change with sediment loss. The sediment losses of Suide soil exhibited the maximum values, whereas the maximum SOC loss occurred on the Yangling soil except on the slope of 25° where the Changwu soil was accompanied with the maximum SOC loss. Therefore, although the sediment loss decided the SOC loss to some extent, the SOC concentration was important for SOC loss. Furthermore, the total sediment loss and total SOC loss for the Suide, Ansai, and Yangling soils exhibited the largest values on the slope of 20°. However, for the Changwu soils, SOC loss increased with the increase in slope angle. The sediment or SOC concentration of different soils varied with slope. However, SOC concentration and SOC loss changed more serious with slope for Ansai and Yangling soils with high aggregate contents than that of Suide and Changwu soils. The sediment concentration of different soils showed a similar change trend to that of total sediment loss.

An exponential relationship existed between the total SOC loss and the median diameter difference of the effective and dispersing sediment particles (δD_{50}) (Fig. 2). δD_{50}, which can represent the soil roughness related to soil erodibility (e.g., aggregate contents) and the SOC content, was also proposed as a variable in our study. With the increase in δD_{50}, total SOC loss increased quickly first and then increased slowly.

3.2. Relationships of sediment and SOC loss to hydraulic factors

The relationships of two primary flow dynamic characteristics (i.e., average flow velocity and runoff depth) and three hydraulic parameters (i.e., shear stress, stream power, and unit stream power) to sediment and SOC loss were analyzed (Table 2). The average flow velocity at the plot was significantly correlated with SOC concentration ($P < 0.01$) but not with SOC loss, sediment concentration, and total sediment loss. Stream power was significantly correlated with SOC concentration ($P < 0.05$) and SOC loss ($P < 0.01$) but not with sediment concentration and total sediment loss. Arjmand and Mahmoodabadi (2015) proposed that all hydraulic characteristic parameters (e.g., stream power, shear

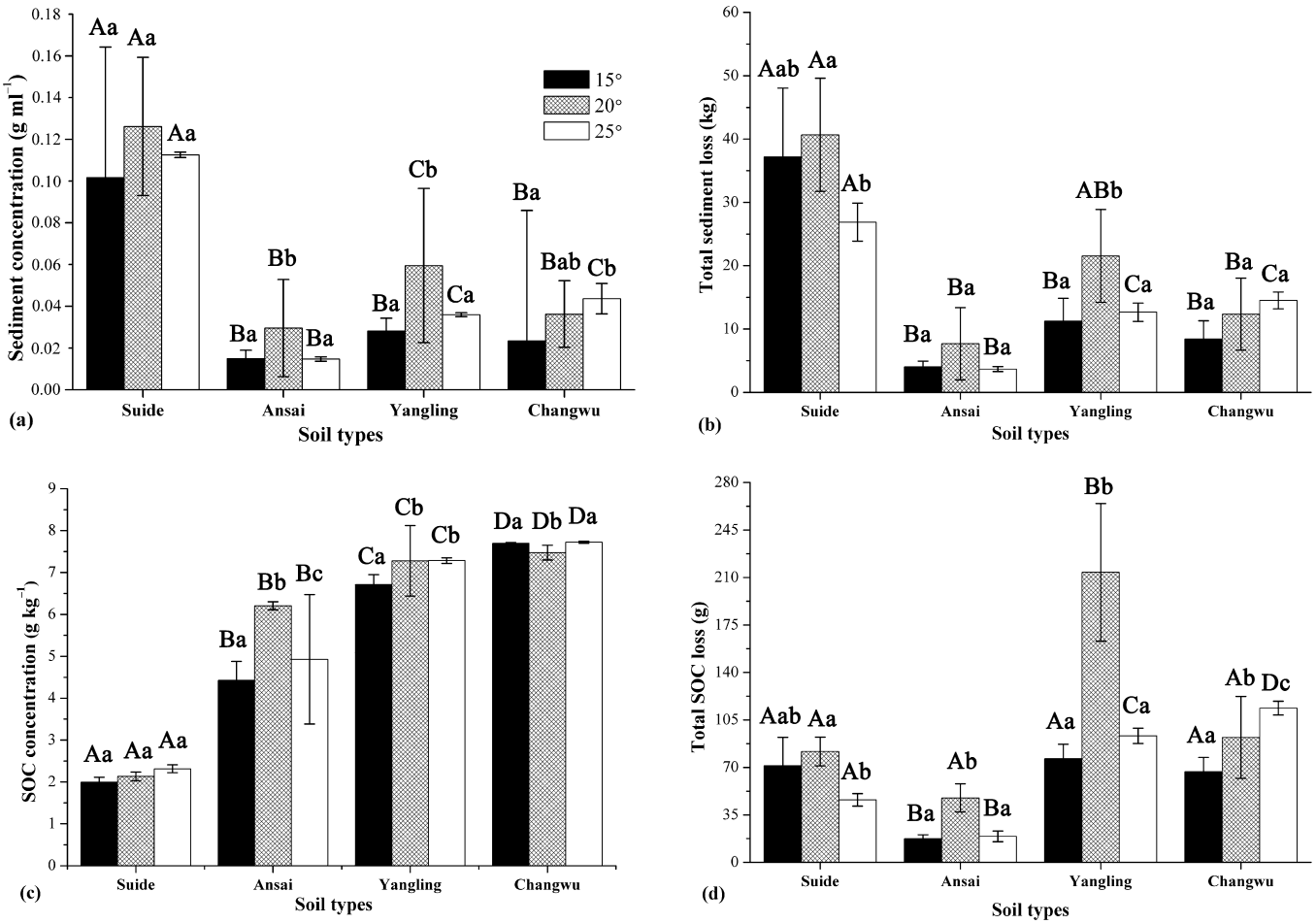

Fig. 1. Sediment concentration, total sediment loss, SOC concentration, and total SOC loss distribution for the Suide, Ansai, Yangling, and Changwu soils at slopes of 15°, 20°, and 25°. (a) Different uppercase letters indicated the significant differences between the treatments with the same slope for the four soils at $P < 0.05$. (b) Different lowercase letters indicated the significant differences between the treatments for one soil at $P < 0.05$.

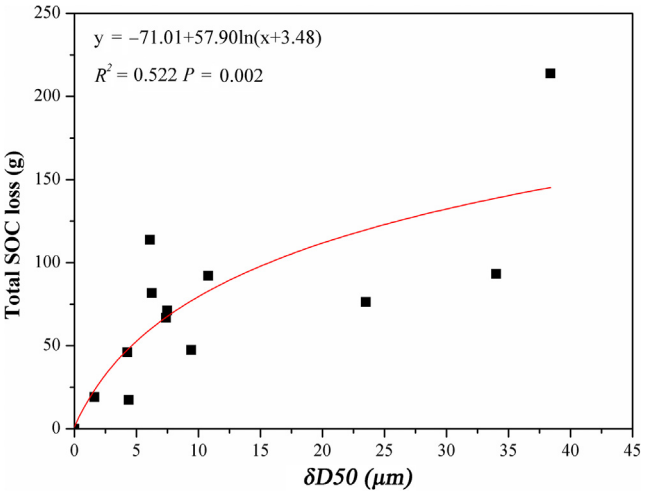

Fig. 2. The relationship of total SOC loss with median diameter difference for the effective and dispersing sediment particles (δD_{50}).

stress, and unit stream power) exhibit significant relationships with sediment concentration, especially flow velocity. However, the runoff depth, shear stress, and unit stream power in our study did not significantly correlate with sediment concentration, total sediment loss, SOC concentration, and total SOC loss.

3.3. Relationship of flow velocity to SOC concentration

PCA was conducted to investigate the mechanism of flow velocity in affecting SOC concentration. Three PCs were extracted from the 11 parameters mentioned above by PCA analysis because the three PCs explained 92.62% of the variability in the original variables (Table 3). The third PC was the uncertainty effect factor or the experimental error. The values of the first PC (PC-1) increased with flow velocity; thus, this PC was defined as the hydraulic factor (Fig. 3). The values of the second PC (PC-2) significantly represented the sediment loss or its related factors (e.g., δD_{50}); thus, this PC was defined as the soil erodibility factor. Fig. 3 shows that the PC-1 values of each soil increased with the SOC concentration in sediments. Meanwhile, the PC-2 values of each soil increased with its SOC loss amounts. Thus, the points of each soil were distributed in different quadrants. Given that the treatment with a slope of 20° was accompanied by a large SOC enrichment ratio, one point separated from the point cloud for Ansai soil. Meanwhile, the points of Yangling soil were scattered from one another because of the significant difference of sediment loss among treatments. The soil erodibility factor that determined sediment loss was a more important effect factor for total SOC loss than the hydraulic factor that decided the SOC concentration, as PC-1 only accounted for 0.493 of total SOC loss and PC-2 accounted for 0.793 of total SOC loss. From PC, SOC concentration was found to also share a close relationship with flow velocity, especially the flow velocity on the 2 m location from the outlet.

Table 2
Correlation relationships of soil loss, SOC loss, flow characteristics (average flow velocity, runoff depth) and hydraulic parameters (shear stress, stream power and unit stream power).

Factors	SC (g ml^{-1})	TSL (kg)	SOCC (g kg^{-1})	Total SOC loss (g)	Slope (m m^{-1})	Averageflow velocity (m s^{-1})	Runoff depth (m)	Shear stress (Pa)	Stream power (W m^{-2})	Unit stream power (m s^{-1})
SC (g ml^{-1})	1	0.942**	−0.662**	0.402	0.028	−0.477	0.173	0.127	−0.286	−0.179
TSL (kg)	0.942**	1	−0.533*	0.566**	−0.100	−0.419	0.402	0.323	−0.079	−0.230
SOCC (g kg^{-1})	−0.662**	−0.533*	1	0.247	0.178	0.899**	−0.045	0.170	0.622**	0.366
Total SOC loss (g)	0.402	0.566**	0.247	1	−0.001	0.540	0.222	0.286	0.434*	0.136
Slope (m m^{-1})	0.028	−0.100	0.178	−0.001	1	0.134	−0.481*	0.134	0.404	0.771**
Average flow velocity (m s^{-1})	−0.477	−0.419	0.899**	0.540	0.134	1	−0.299	−0.022	0.592*	0.544
Runoff depth (m)	0.173	0.402	−0.045	0.222	−0.481*	−0.299	1	0.780**	0.215	−0.641**
Shear stress (Pa)	0.127	0.323	0.170	0.286	0.134	−0.022	0.780**	1	0.611**	−0.160
Stream power (W m^{-2})	−0.286	−0.079	0.622**	0.434*	0.404	0.592*	0.215	0.611**	1	0.547*
Unit stream power (m s^{-1})	−0.179	−0.230	0.366	0.136	0.771**	0.544	−0.641**	−0.160	0.547*	1

SC: sediment concentration; TSL: total sediment loss; SOCC: SOC concentration; Average flow velocity: average flow velocity of the four locations on the plot.
** Correlation is significant at the 0.01 level (two-tailed).
* Correlation is significant at the 0.05 level (two-tailed).

Table 3
Rotated principal component (PC) pattern for soil and SOC loss and its related factors for Suide, Ansai, Yangling, and Changwu soils (n = 24).

Variables	PC 1[a] (Hydraulic factors)	PC 2[a] (Soil erodibility)	PC 3[a] (others)
SC (g ml^{-1})	**−0.632**	**0.649**	0.403
TSL (kg)	−0.570	**0.711**	0.368
SOCC (g kg^{-1})	**0.967**	−0.140	−0.107
Total SOC loss (g)	0.493	**0.762**	0.010
EMD (μm)	−0.369	**0.806**	−0.339
δD_{50} (μm)	0.523	**0.651**	−0.532
Flow velocity (1 m) (m s^{-1})	**0.880**	0.347	0.145
Flow velocity (2 m) (m s^{-1})	**0.965**	−0.045	-0.128
Flow velocity (3 m) (m s^{-1})	**0.947**	0.052	0.287
Flow velocity (4 m) (m s^{-1})	**0.830**	−0.020	0.486
SOC enrichment	**0.846**	0.281	0.041
Explained variance (%)	57.44	25.50	9.68

SC: sediment concentration; TSL: total sediment loss; SOCC: SOC concentration; EMD: effective median diameter; δD_{50}: median diameter difference for the effective and dispersing sediment particles.
[a] Values in bold have a loading of 0.6 or higher and contribute strongly to the PC.

Significant linear relationships between flow velocity and SOC concentration were observed ($R^2 > 0.467$ and $P < 0.01$) (Fig. 4). The flow velocity at the 2 m location from the outlet exhibited the most important relationship with SOC concentration ($R^2 = 0.893$ and $P < 0.001$). Nonparametric scatter plot matrix of the soil particle distribution (clay, fine silt, coarse silt, and sand) and flow velocities at different locations of the plot were obtained by Pearson correlation analysis to further investigate the internal mechanism of the effect of flow velocity on SOC concentration (Fig. 5). Fig. 5 shows that average flow velocities showed positive correlation with the clay and fine silt contents in sediments ($P < 0.01$), especially the average flow velocity at 2 m location from the outlet. Conversely, average flow velocities exhibited negative correlations with coarse silt, fine sand, and coarse sand contents ($P < 0.05$). Meanwhile, SOC concentration presented significant positive exponential relationship with clay and silt contents ($R^2 = 0.951$ and $P < 0.001$, Fig. 6). Clay and silt usually combine with SOM (Leifeld et al., 2005; Meersmans et al., 2008). Therefore, we concluded that the selective transport of clay and silt controlled by flow velocity resulted in the correlation of flow velocity and SOC concentration.

The average flow velocity at the low and middle parts of hill slope showed a significant relationship with SOC loss whereas that at the foot of hill slope did not. To investigate the reason for this result, we compared flow velocities under a perfect smoothing slope without erosion with flow velocities in an actual erosion situation. In a perfect situation, the increased rate of flow velocity decreases with distance from the plot top. However, the increased rate of flow velocity increased with distance during erosion in our study (Fig. 7). This phenomenon was due to that significant rill erosion occurred at the 3 m location and the sediment runoff was under transport-limiting conditions. Li et al. (2016a) certified that heavy erosion occurs in the upper- and lower-middle regions of slope. Therefore, the flow velocity at the location of the hill slope where maximum sediment load was attained for runoff could be regarded as the representative factor for the SOC concentration for the loess soils.

3.4. Sediment loss prediction

Under high-rainfall intensity, WEPP cannot perfectly predict the sediment loss on steep slopes when complex serious erosion occurs, such as gravitational erosion, ephemeral gully, and gully erosion, especially in China (Zheng, 2006). Referring to the estimation of sediment loss in process-based models (e.g., WEPP) and considering the hydraulic mechanism accompanied with soil erosion, sediment loss could be calculated by a hydraulic-based sediment empirical model even with the occurrence of serious erosion, as shown in Eq. (9). To understand the model easily, bulk density for each soil and correction coefficient (1000) were incorporated into the erosion model. Parameters a, b, and c for the Suide, Ansai, Yangling, and Changwu soils were preliminary calculated by nonlinear regression. The regression results are shown in Table 4.

3D scatter plots were provided for further investigating the effect of δD_{50} and SOC content on SOC loss (Fig. 8). We found that δD_{50} of the original soil affected E_s by controlling V. SOC content also affected E_s by controlling S. These conditions illustrated that δD_{50} and SOC content decided the contribution of flow velocity and slope to total sediment loss, respectively. Then, parameters a and b showed significant positive exponential and logarithmic relationships with δD_{50}, respectively (Fig. 9). Parameter c displayed a significant negative exponential relationship with the SOC content of the original soil. Therefore, we proposed that parameters a, b, and c could be predicted by δD_{50} or the SOC content of the original soil. The formulas are shown in Eqs. (10)–(12). The regression coefficients and its error are shown in Table 5. After building the

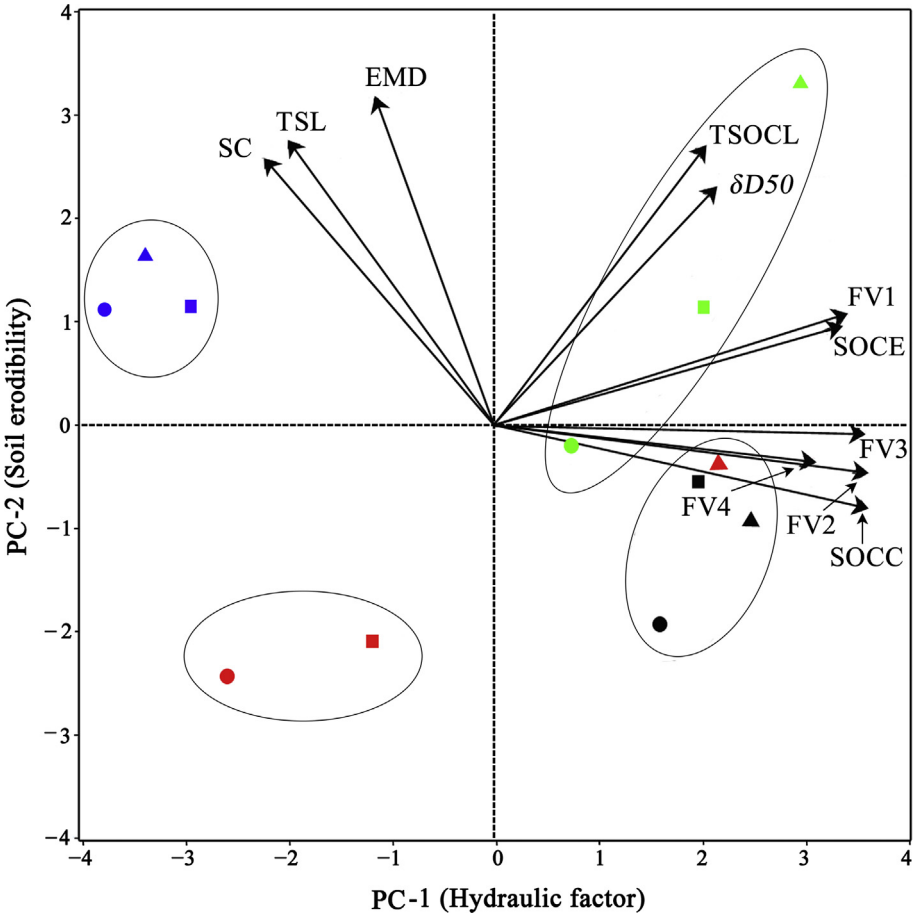

Fig. 3. Biplot for principal component (PC-1) (hydraulic factor) and principal component (PC-2) (soil erodibility). The scores of the Suide, Ansai, Yangling, and Changwu are displayed for the three slopes: 15° (●), 20° (▲), and 25° (■). The colors represent various soils: Suide (blue in web version), Ansai (red in web version), Yangling (green in web version), and Changwu (black in web version). The factor loadings are represented by the black vectors. The short names were shown as follows: SC: Sediment concentration; TSL: Total sediment loss; SOCC: SOC concentration; TSOCL: Total SOC loss; SOCE: SOC enrichment; EMD: Effective median diameter of sediment particles; δD_{50}: Median diameter difference between effective and dispersing sediment particles; FV1, 2, 3 or 4: Average flow velocity at the 1 m, 2 m, 3 m or 4 m location from outlet.

model, its evaluation was conducted; the input variables are shown in Table 6. Model parameters *a*, *b* and *c* were recalculated by entering the values of δD_{50} and SOC content into Eqs. (10)-(12). The calculated parameters were reentered into the proposed erosion model. Sediment loss was predicted by entering the values of runoff rate, flow velocity, and slope into the model. All predicted values could be fitted well with the measured ones (Fig. 10). However, the sediment model exhibited better performance for the Suide and Changwu soils ($R^2 > 0.905$, and $d > 0.977$) than for the Ansai and Yangling soils ($R^2 > 0.410$ and $d > 0.822$) (Table 7). In fact, the aggregate contents for the Ansai and Yangling soils were higher than those for the Suide and Changwu soils.

3.5. SOC loss prediction

The mechanism of flow velocity in controlling SOC concentration was investigated in our study for loess soils. Meanwhile, stream power was found correlated to SOC loss. However, SOC loss is usually estimated by sediment loss (Häring et al., 2014; Li et al., 2016c). Therefore, a similar hydraulic-based SOC loss model was proposed, as shown in Eq. (13), by incorporating the SOC content into the erosion model. In fact, SOC content variable (C_{soc}), which can be predicted by flow velocity, is not the essential variable and can be ignored if necessary without reducing the model prediction accuracy. Parameters *a*, *b*, and *c* of the SOC loss model were also calculated by nonlinear regression (Table 4). The parameters also showed the same regular relationships with δD_{50} or SOC content as obtained by the above-mentioned method (Fig. 8). The relationships between parameters *a*, *b*, and *c* and δD_{50} or SOC content could also be nonlinearly regressed by Eqs. (10)-(12) (Fig. 9). The regression results and regression accuracy are shown in Table 5 ($R^2 > 0.932$ and $P < 0.05$).

Parameters *a*, *b*, and *c* of the SOC loss model were recalculated by entering the values of δD_{50} and SOC content into Eqs. (10)–(12). The prediction accuracy of the SOC loss model was estimated, as shown in Fig. 10 and Table 7. The prediction accuracy for four soils with different soil textures was similar to that of the erosion model. The SOC model also exhibited better performance for the Suide and Changwu soils ($R^2 > 0.903$, and $d > 0.974$) than for the Ansai and Yangling soils with high aggregate contents ($R^2 > 0.496$, and $d > 0.861$). The aggregates concentrated on the same soil particle grade for different loess soils (Wang and Shi, 2015); thus, δD_{50} could represent the aggregate content. The effect of flow velocity on sediment or SOC loss increased with the increase in aggregate content in soils as obtained by the model. The effect of slope on sediment or SOC loss decreased as SOC content increased.

4. Discussion

4.1. Hydraulic factors and sediment and SOC loss

Among the hydraulic factors, average flow velocity showed close correlations with SOC concentration, whereas stream power

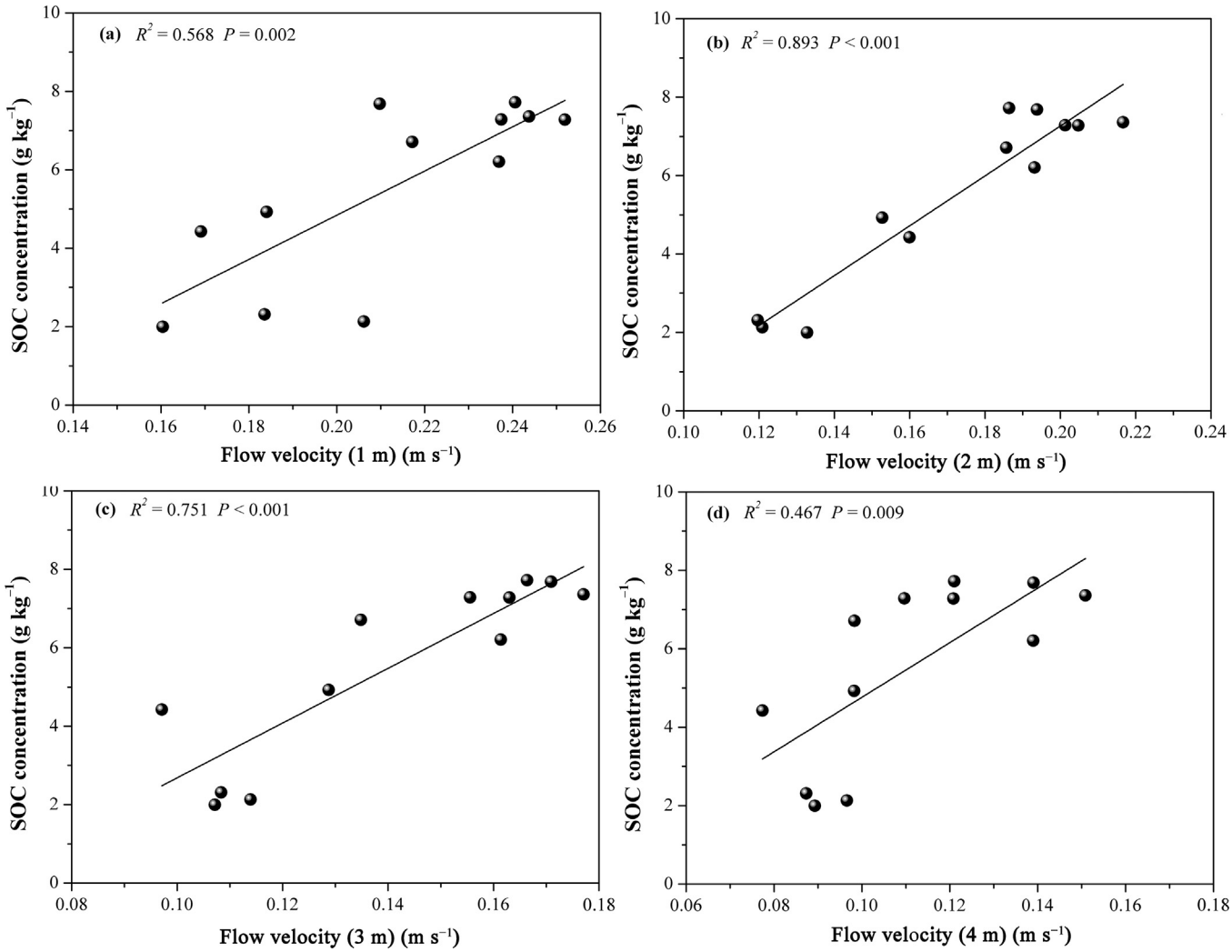

Fig. 4. Relationships of the average flow velocity at 1, 2, 3, and 4 m from the outlet to the SOC concentration.

was closely related to SOC concentration and SOC loss. Shi et al. (2012) noted that different sediment transports [i.e., suspended, saltating, and contact (rolling) loads] are normally broadly associated with particular sediment size ranges. From our study, the organic carbons were found mainly bonded with clay and silt particles in sediments, which were easily transported by suspension–saltation transport of overland flow (Shi et al., 2012). A positive correlation between SOC content and clay content is previously observed (Leifeld et al., 2005; Meersmans et al., 2008). A positive correlation between clay and silt content and flow velocity was also found in our study. We concluded that flow velocity controlled SOC enrichment by increasing the amount of clay particles in sediments; this deduction was possible because the smallest particles (< 0.005 mm) were easily transported by overland flow (Rodriguez et al., 2002; Starr et al., 2000; Swanson and Dedrick, 1967). Thus, suspension–saltation transport of loess soils was mainly related to flow velocity. Some clay-sized particles are usually transported as aggregates (Wang and Shi, 2015), and stream power generally exhibits a close relationship with the relative effect of sediment transport by contact (rolling) load (Shi et al., 2012). From our study, SOC loss was found to present a close relationship with δD_{50}, which could represent aggregate contents for loess soils. In fact, water-stable macroaggregation is also an important determining factor of erodibility (Barthès et al., 1999). Therefore, stream power and δD_{50} were found correlated with SOC loss in our study. The enrichment of organic carbon in sediments is generally attributed to the preferential transportation of poorly decomposed noncohesive plant fragments or fine-sized sediments (Li et al., 2016b). The SOC enrichment of loess soils in our study was due to the increase in the amounts of small sediment particles and clay-comprised aggregates. SOC usually combines with clay particles and is the most stably sized fraction in soils (Anderson et al., 1981; Starr et al., 2000). In our study, clay particles were first transported for the loess soil; thus, SOC loss amount could seriously affect the loess soil as a carbon sink (De et al., 2015; Ma et al., 2014).

All findings and conclusions about the hydraulic mechanism of SOC transport were investigated under short-high rainfall intensity. The relationships of hydraulic factors and SOC loss should be further investigated under small rainfall intensity. Meanwhile, the hydraulic mechanism controlling SOC enrichment ratio should also be further investigated for other soils and large scales.

4.2. Simple sediment and SOC loss model

Referring to previous physical-based model and the relationship between flow velocity and SOC concentration, a hydraulic-based soil and SOC loss empirical model was proposed in our study. Model parameters were related to δD_{50} or the SOC content of the original soil because of the effect of the hydraulic roughness and

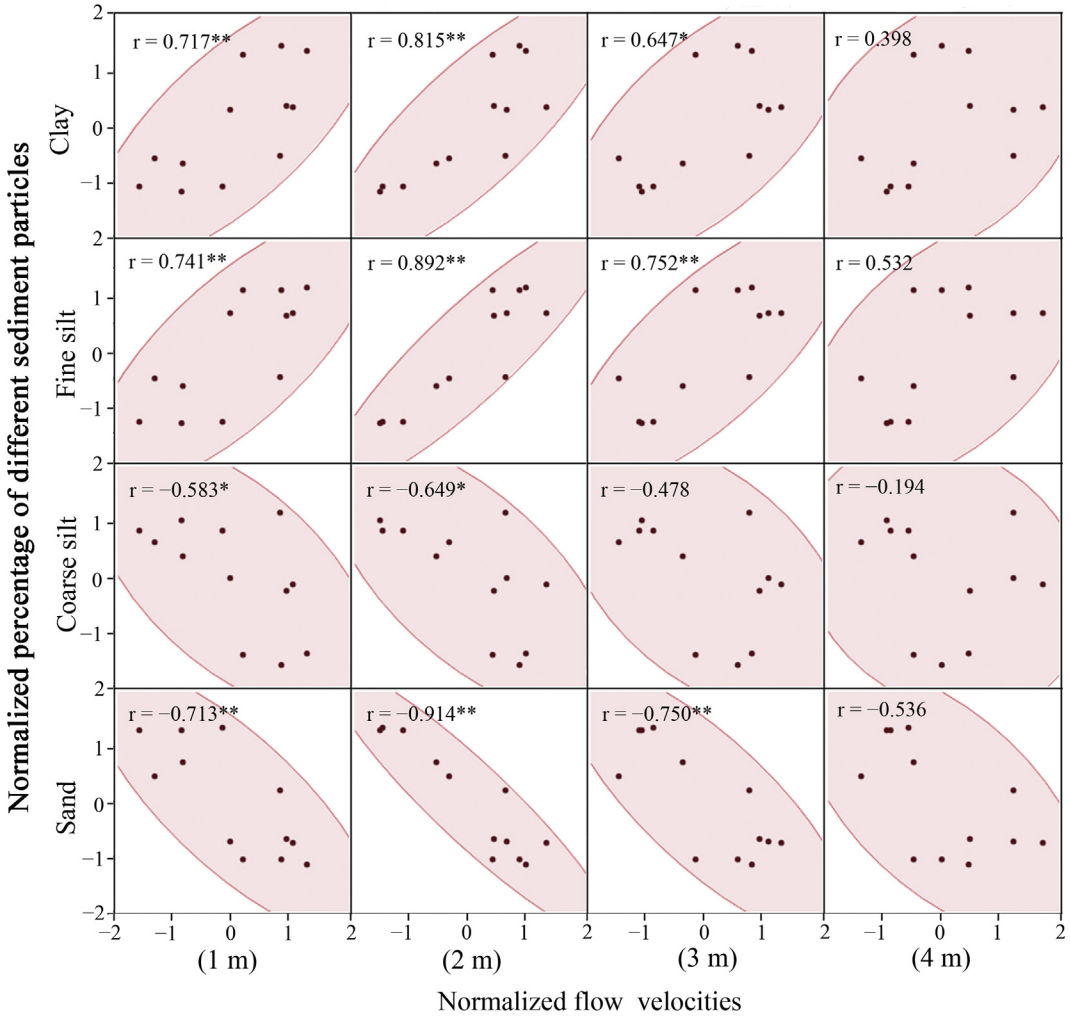

Fig. 5. Scatter plot map of normalized different sediment particles contents and normalized average flow velocities at the four locations (1, 2, 3, and 4 m) from the outlet [Soil texture is classified on the basis of the USDA soil classification system; ** Correlation is significant at the 0.01 level (two-tailed); * Correlation is significant at the 0.05 level (two-tailed)].

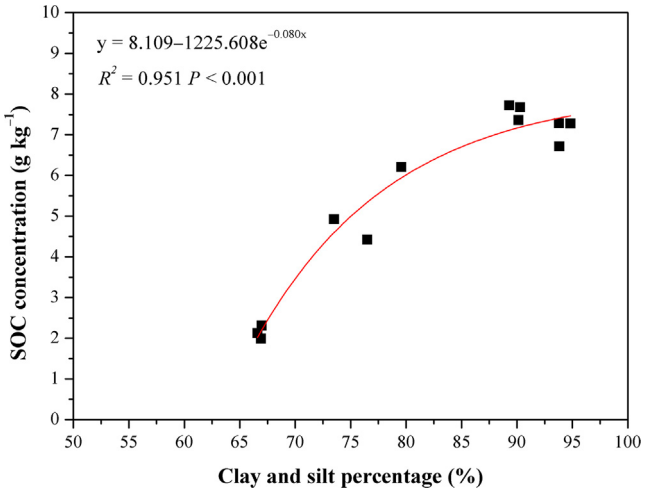

Fig. 6. The exponential relationship of SOC concentration with clay and silt percentage in sediments.

the median particle size of the soil on sediment loss (Quinton et al., 2006). In our study, aggregate content exhibited obvious effect on model accuracy. The soils with low aggregate content were better predicted than the ones with high-aggregate content. Our proposed model mainly focused on the sediment loss during serious erosion on the Loess Plateau. Although the empirical model could not predict the sediment loss at any hill slope location, it could effectively predict the sediment loss for the cases that could not be addressed using physical-based models (Wang et al., 2007).

Rainfall intensity affected the erosion process mainly by controlling the hydraulic process on slope (Kinnell, 2005). Rill erosion mainly occurred during the flow detachment with transport by flow period when transport mechanism of suspension and rolling was more important than saltation. Although rainfall intensity is important on the conversion between raindrop detachment/splash erosion and flow detachment/flow erosion, transport mechanisms decided the application of our proposed model. Therefore, the effect of varying high-rainfall intensity was not also considered in our studies. In addition, as the submodel of SOC dynamic model, SOC loss was mainly predicted by the sediment loss for large-scale or long-time scale in previous studies (Häring et al., 2014; Li et al., 2016c). Field monitoring under simulated rainfall conditions is a good method to develop diagnostic models and to study the hydraulic effects (Cao et al., 2015; Foltz et al., 2009). Meanwhile, the same calculation method may be effectively used for the calculation of soil and SOC loss on gauging station at small catchment

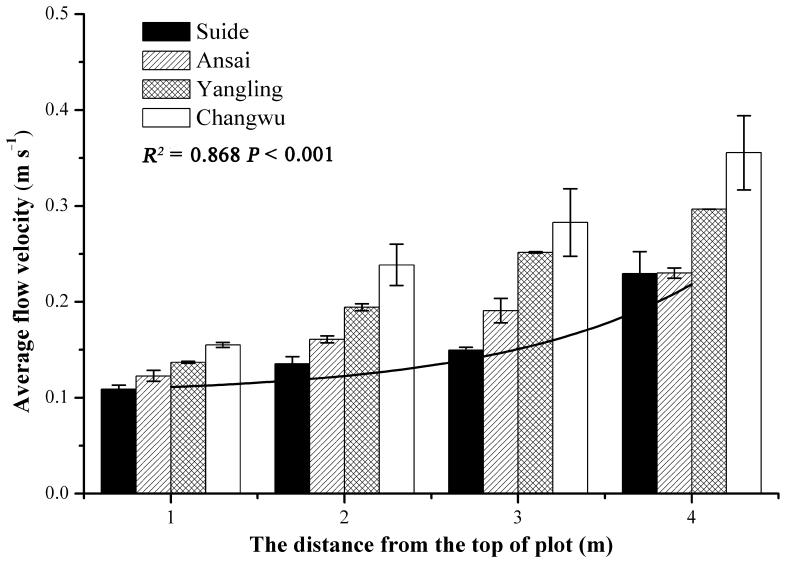

Fig. 7. Trend of the average flow velocity with the increase in the distance from the top of the plot to the measurement location (an example at the slope of 25° for the four soils) (Means ± RMSE).

Table 4
Model parameters for the sediment and SOC loss prediction model for the Suide, Ansai, Yangling, and Changwu soils.

Soil types	Parameters-sediment			Parameters-SOC		
	a	*b*	*c*	a_o	b_o	c_o
Suide	0.046	−0.934	0.758	0.090	−0.774	1.070
Ansai	1.486 E−11	−4.290	0.132	3.428 E−5	−4.243	0.630
Yangling	3.601 E7	16.018	−1.593	7.530 E7	16.320	−1.485
Changwu	0.119	3.863	−3.666	0.150	3.946	−3.715

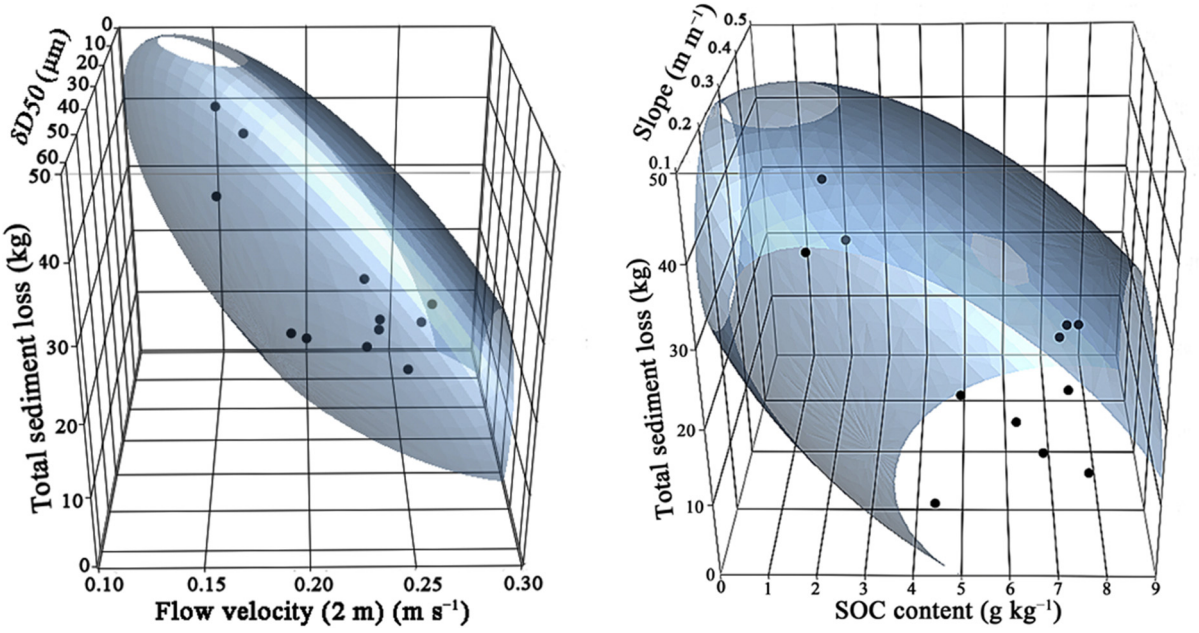

Fig. 8. The three-dimensional (3D) scatter plot fitted by ellipsoid of δD_{50}, flow velocity at 2 m to the outlet and total sediment loss, and SOC content, slope and total sediment loss.

scale. Therefore, hydraulic-based SOC model can bring a new important reference for the SOC prediction. However, under the low rainfall intensity, a physical-based model may exhibit a good prediction accuracy when erosion is not serious. Finally, by this method, hydraulic-based sediment or SOC loss empirical model for severe erosion for different soils may also be built.

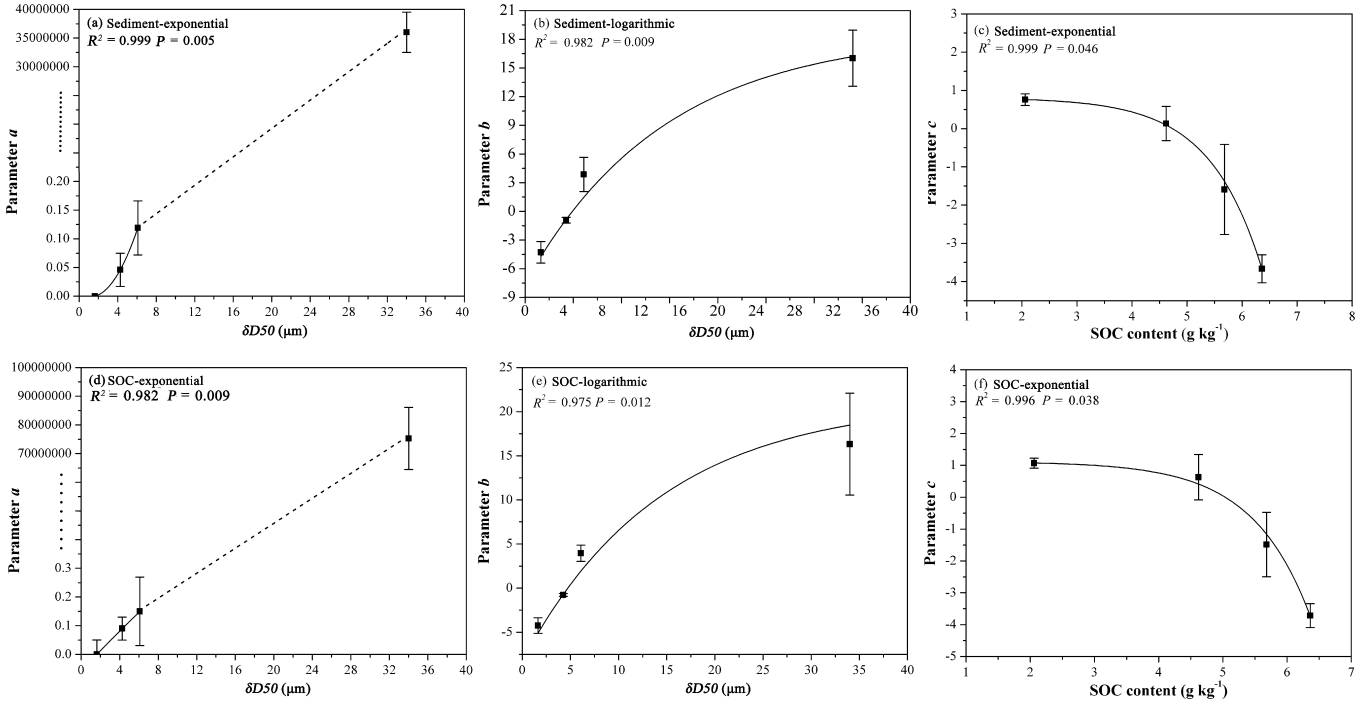

Fig. 9. Relationships between the parameters (a, b, and c) and δD_{50} or SOC content for the Suide, Ansai, Yangling, and Changwu soils.

Table 5
Regression coefficients and statistical indices for the relationships between model parameters and δD_{50} or SOC content of original soils.

Model parameters	Coefficients-sediment			Agreement index-Sediment	
	y0	*A*	*k*	R^2	*P*
a	0.002 ± 0.011	0.002 ± 0.000	0.700 ± 0.006	1.000	0.001
b	−8.912 ± 2.400	6.918 ± 1.130	1.000 ± 0.000	0.974	0.009
c	0.836 ± 0.103	−0.008 ± 0.000	1.000 ± 0.000	0.999	0.046
	Coefficients-SOC			Agreement index-SOC	
a_o	0.019 ± 0.036	−0.002 ± 0.002	0.721 ± 0.721 m	1.000	0.009
b_o	−8.912 ± 2.343	6.999 ± 1.103	1.000 ± 0.000	0.932	0.012
c_o	1.255 ± 0.261	−0.009 ± 0.001	1.00 ± 0.000	0.996	0.038

Table 6
Input values [Flow velocity at the 2 m location from outlet, runoff rate and median diameter difference of the effective and dispersing soil particles (δD_{50})] of the model.

Soil types	Average flow velocity (2 m) at different slopes (m s^{-1})			Average runoff rate at different slopes (ml s^{-1})			δD_{50}
	15°	20°	25°	15°	20°	25°	
Suide	0.17	0.15	0.15	85.89	72.11	34.91	4.27
Ansai	0.20	0.24	0.19	96	83.69	73.47	1.63
Yangling	0.23	0.26	0.25	110.39	108.75	109.44	34.00
Changwu	0.24	0.27	0.23	70.83	100.92	93.89	6.09

5. Conclusion

To improve the prediction accuracy of sediment and SOC loss accompanied with complex serious erosion, an empirical sediment and SOC model was proposed. The results showed that the flow velocity, especially the flow velocity at the location where the runoff was transport limited, exhibited direct effect on SOC concentration by controlling selective transport of the fine particles. When runoff rate, slope, flow velocities, δD_{50}, and SOC content served as input variables, a hydraulic-based empirical model was built. In the model, δD_{50} and SOC content were used to determine the parameters of the master equation of the model. The proposed model shows good prediction accuracy even if rill morphology and other erosion processes suffer complex changes. However, high-aggregate contents decreased the prediction accuracies of the proposed sediment and SOC model. From the model, aggregate contents exhibit positive effect on the contribution of flow velocity to sediment or SOC loss, whereas SOC content displays negative effect on the slope contribution. Considering that our study mainly focused on the loess soils, similar model may be built for other soils, which need to be further investigated. Overall, the applicability of the newly proposed models will serve as an important reference for WEPP and the SOC dynamic model.

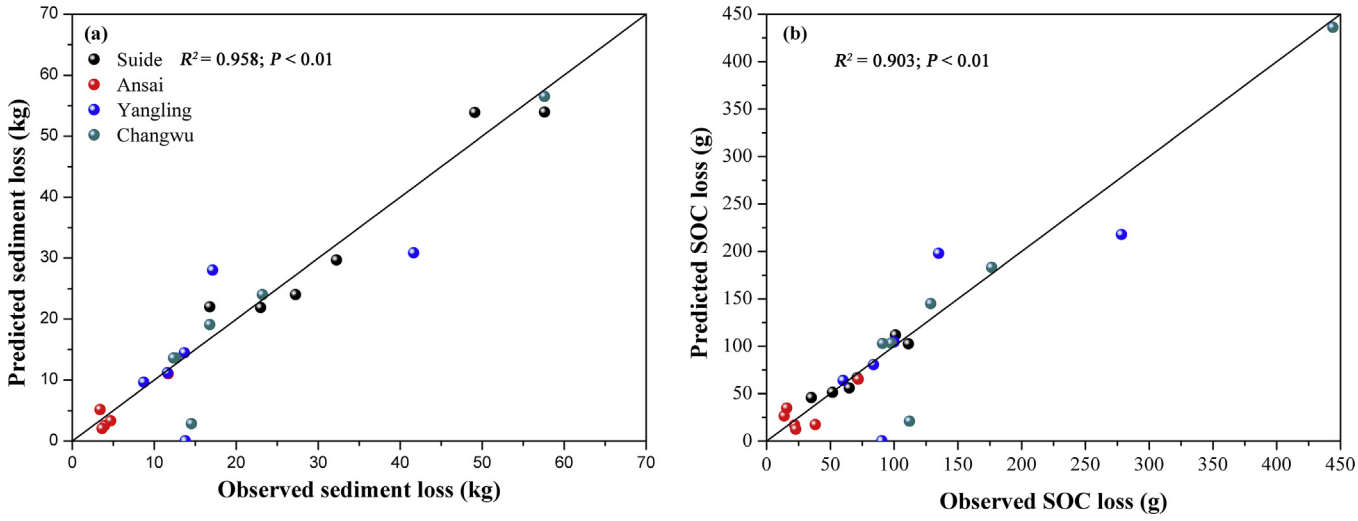

Fig. 10. Map plots of the measured sediment loss and the predicted sediment loss (a), and the measured total SOC loss and the predicted total SOC loss (b) for the Suide, Ansai, Yangling, and Changwu soils.

Table 7
Statistical indices for the sediment and SOC loss prediction model for the Suide, Ansai, Yangling, and Changwu soils.

Soil types	Agreement index-sediment		
	RMSE	R^2	d
Suide	3.694	0.935.	0.983
Ansai	1.470	0.756	0.936
Yangling	8.428	0.410	0.822
Changwu	4.927	0.905	0.977
	Agreement index-SOC		
Suide	8.233	0.903	0.974
Ansai	13.750	0.526	0.861
Yangling	51.302	0.496	0.866
Changwu	38.371	0.903	0.977

Acknowledgment

This study was financially supported by the "Hundred-Talent Project" of the Chinese Academy of Sciences and the National Natural Science Foundation of China (41271294).

Appendix A. Supplementary data

Supplementary data associated with this article can be found, in the online version, at https://doi.org/10.1016/j.jhydrol.2017.09.010. These data include Google maps of the most important areas described in this article.

References

Abdi, H., Williams, L.J., 2010. Principal component analysis. WIREs Comput. Stat. 2 (4), 433–459.
Anderson, D.W., Saggar, S., Bettany, J.R., Stewart, J.W.B., 1981. Particle size fractions and their use in studies of soil organic matter: I. The nature and distribution of forms of carbon, nitrogen, and sulfur. Soil Sci. Soc. Am. J. 45, 767–772.
Arjmand, S.S., Mahmoodabadi, M., 2015. Sediment concentration and hydraulic characteristics of rain-induced overland flows in arid land soils. J. Soil Sediments 15 (3), 710–721.
Armentano, M.G., Christensen, I., Schiaffino, S., 2015. Applying the technology acceptance model to evaluation of recommender systems. Polibits 51, 73–79.
Avnimelech, Y., McHenry, J.R., 1984. Enrichment of transported sediments with organic carbon, nutrients, and clay. Soil Sci. Soc. Am. J. 48, 259–266.
Barthès, B., Albrecht, A., Asseline, J., De Noni, G., Roose, E., 1999. Relationship between soil erodibility and topsoil aggregate stability or carbon content in a cultivated mediterranean highland (Aveyron, France). Commun. Soil Sci. Plant Anal. 30 (13–14), 1929–1938.
Berhe, A.A., Kleber, M., 2013. Erosion, deposition, and the persistence of soil organic matter: mechanistic considerations and problems with terminology. Earth Surf. Proc. Land. 38 (8), 908–912.
Cai, Q., Wang, G., Chen, Y., 1998. The critical condition and sediment yielding of rill erosion. In: Process of Sediment Yield in a Small Watershed of the Loess Plateau and its Modeling. Sci. Press, p. Beijing. 92–103 (In Chinese).
Cao, L., Liang, Y., Wang, Y., Lu, H., 2015. Runoff and soil loss from Pinus massoniana forest in southern China after simulated rainfall. Catena 129, 1–8.
Chen, Y.Z., 1987. A review: the study of soil erosion on Loess Plateau. Geogr. Res. 6, 76–85 (In Chinese).
Comprehensive Scientific Expedition, C.M., 1990. Slope classification data set of cultivated land on Loess Plateau area. Nat. Sci. Technol. Infrastructure China, Data Sharing Infrastructure Earth Syst. Sci., Chinese Acad. Sci., Beijing. http://www.geodata.cn.
De, C.T., Heiling, M., Dercon, G., Resch, C., Aigner, M., Mayer, L., Mao, Y., Elsen, A., Steier, P., Leifeld, J., Merckx, R., 2015. Predicting soil organic matter stability in agricultural fields through carbon and nitrogen stable isotopes. Soil Biol. Biochem. 88, 29–38.
De Roo, A.P.J., Wesseling, C.G., Ritsema, C.J., 1996. LISEM: a single-event physically based hydrological and soil erosion model for drainage basins. I: theory, input and output. Hydrol. Process. 10 (8), 1107–1117.
Finkner, S.C., Gilley, J.E., 1988. Measurement of flow components on upland areas using dye dilution techniques. Trans. ASAE 31 (4), 1086–1091.
Foltz, R.B., Copeland, N.S., Elliot, W.J., 2009. Reopening abandoned forest roads in northern Idaho, USA: quantification of runoff, sediment concentration, infiltration, and interrill erosion parameters. J. Environ. Manage. 90 (8), 2542–2550.
Foster, G.R., Flanagan, D.C., Nearing, M.A., Lane, L.J., Risse, L.M., Finker, S.C., 1995. Hillslope erosion component. In: Flanagan, D.C., Nearing, M.A. (Eds.), USDA-Water Erosion Prediction Project Hillslope Profile and Watershed Model Documentation. USDA, Indiana, pp. 11.1–11.12.
Fu, B., 1989. Soil erosion and its control in the Loess Plateau of China. Soil Use Manage. 5 (2), 76–82.
Gilley, J.E., Kottwitz, E.R., Simanton, J.R., 1990. Hydraulic characteristics of rills. Trans. ASAE 33 (6), 1900–1906.
Govers, G., 1990. Empirical Relationships for the Transport Capacity of Overland Flow. vol. 189, IAHS publ., 45–63.
Gregorich, E.G., Gillespie, A.W., Beare, M.H., Curtin, D., Sanei, H., Yanni, S.F., 2015. Evaluating biodegradability of soil organic matter by its thermal stability and chemical composition. Soil Biol. Biochem. 91, 182–191.
Häring, V., Fischer, H., Cadisch, G., Stahr, K., 2013. Implication of erosion on the assessment of decomposition and humification of soil organic carbon after land use change in tropical agricultural systems. Soil Biol. Biochem. 65, 158–167.
Häring, V., Fischer, H., Stahr, K., 2014. Erosion of bulk soil and soil organic carbon after land use change in northwest Vietnam. Catena 122, 111–119.
Hessel, R., Jetten, V., 2007. Suitability of transport equations in modelling soil erosion for a small Loess Plateau catchment. Eng. Geol. 91 (1), 56–71.
Kinnell, P.I.A., 2005. Raindrop-impact-induced erosion processes and prediction: a review. Hydrol. Process. 19 (14), 2815–2844.
Lal, R., 2003. Soil erosion and the global carbon budget. Environ. Int. 29 (4), 437–450.
Lal, R., 2005. Soil erosion and carbon dynamics. Soil Till. Res. 81 (2), 137–142.
Leifeld, J., Bassin, S., Fuhrer, J., 2005. Carbon stocks in Swiss agricultural soils predicted by land-use, soil characteristics, and altitude. Agr. Ecosyst. Environ. 105 (1–2), 255–266.

Li, Z., Liu, C., Dong, Y., Chang, X., Nie, X., Liu, L., Xiao, H., Lu, Y., Zeng, G., 2017. Response of soil organic carbon and nitrogen stocks to soil erosion and land use types in the Loess hilly–gully region of China. Soil Till. Res. 166, 1–9.
Li, Z., Lu, Y., Nie, X., Huang, B., Ma, W., Liu, C., Xiao, H., 2016a. Variability of Beryllium-7 and Its potential for documenting soil and soil organic carbon redistribution by erosion. Soil Sci. Soc. Am. J. 80 (3), 693.
Li, Z., Nie, X., Chang, X., Liu, L., Sun, L., 2016b. Characteristics of soil and organic carbon loss induced by water erosion on the Loess Plateau in China. PLoS One 11 (4), e0154591.
Li, Z.W., Liu, L., Nie, X.D., Chang, X.F., Liu, C., Xiao, H.B., 2016c. Modeling soil organic carbon loss in relation to flow velocity and slope on the Loess Plateau of China. Soil Sci. Soc. Am. J. 80 (5), 1341.
Liu, C., Dong, Y., Li, Z., Chang, X., Nie, X., Liu, L., Xiao, H., Bashir, H., 2017. Tracing the source of sedimentary organic carbon in the Loess Plateau of China: an integrated elemental ratio, stable carbon signatures, and radioactive isotopes approach. J. Environ. Radioact. 167, 201–210.
Ma, W., Li, Z., Ding, K., Huang, J., Nie, X., Zeng, G., Wang, S., Liu, G., 2014. Effect of soil erosion on dissolved organic carbon redistribution in subtropical red soil under rainfall simulation. Geomorphology 226, 217–225.
Mahmoodabadi, M., Ghadiri, H., Rose, C., Yu, B., Rafahi, H., Rouhipour, H., 2014. Evaluation of GUEST and WEPP with a new approach for the determination of sediment transport capacity. J. Hydrol. 513, 413–421.
McHugh, M., Wood, G., Walling, D., Morgan, R., Zhang, Y., Anthony, S., Hutchins, M., 2002. Prediction of Sediment Delivery to Watercourses from Land Phase II. Environment Agency R&D Technical report P2-209, Bristol, p. 106.
Meersmans, J., De Ridder, F., Canters, F., De Baets, S., Van Molle, M., 2008. A multiple regression approach to assess the spatial distribution of Soil Organic Carbon (SOC) at the regional scale (Flanders, Belgium). Geoderma 143 (1–2), 1–13.
Meyers, L.S., Gamst, G., Guarino, A.J., 2006. Applied Multivariate Research: Design and Interpretation. Sage Publications, Thousand Oaks, CA. 465–513.
Morgan, R.P.C., Quinton, J.N., Smith, R.E., Govers, G., Poesen, J.W.A., Auerswald, K., Chisci, G., Torri, D., Styczen, M.E., 1998. The European Soil Erosion Model (EUROSEM): a dynamic approach for predicting sediment transport from fields and small catchments. Earth Surf. Proc. Land. 23 (6), 527–544.
Nadeu, E., Van Oost, K., Boix-Fayos, C., de Vente, J., 2014. Importance of land use patterns for erosion-induced carbon fluxes in a Mediterranean catchment. Agr. Ecosyst. Environ. 189, 181–189.
Nash, J.E., Sutcliffe, J.V., 1970. River flow forecasting through conceptual models: 1. A discussion of principles. J. Hydrol. 10, 282–290.
Nearing, M.A., Foster, G.R., Lane, L.J., Finkner, S.C., 1989. A process-based soil erosion model for USDA-Water Erosion Prediction Project technology. Trans. ASAE 32 (5), 1587–1593.
Nearing, M.A., Norton, L.D., Bulgakov, D.A., Larionov, G.A., West, L.T., Dontsova, K.M., 1997. Hydraulics and erosion in eroding rills. Water Resour. Res. 33 (4), 865–876.
Palis, R., Ghandiri, H., Rose, C., Saffigna, P., 1997. Soil erosion and nutrient loss. III. Changes in the enrichment ratio of total nitrogen and organic carbon under rainfall detachment and entrainment. Aust. J. Soil Res. 35 (4), 891–905.
Pan, C., Shangguan, Z., 2006. Runoff hydraulic characteristics and sediment generation in sloped grassplots under simulated rainfall conditions. J. Hydrol. 331 (1–2), 178–185.
Parton, W.J., Schimel, D.S., Cole, C.V., Oiima, D.S., 1987. Analysis of factors controlling soil organic matter levels in great plains grasslands. Soil Sci. Soc. Am. J. 51, 1173–1179.
Planchon, O., Silvera, N., Gimenez, R., Favis-Mortlock, D., Wainwright, J., Bissonnais, Y.L., Govers, G., 2005. An automated salt-tracing gauge for flow-velocity measurement. Earth Surf. Proc. Land. 30 (7), 833–844.
Polyakov, V.O., Lal, R., 2008. Soil organic matter and CO2 emission as affected by water erosion on field runoff plots. Geoderma 143 (1–2), 216–222.
Polyakov, V., Lal, R., 2004. Modeling soil organic matter dynamics as affected by soil water erosion. Environ Int. 30 (4), 547–556.
Prokop, P., Poręba, G.J., 2012. Soil erosion associated with an upland farming system under population pressure in Northeast India. Land Degrad. Dev. 23, 310–321.
Quinton, J.N., Catt, J.A., Wood, G.A., Steer, J., 2006. Soil carbon losses by water erosion: experimentation and modeling at field and national scales in the UK. Agr. Ecosyst. Environ. 112 (1), 87–102.
Rodriguez, A., Guerrra, J.A., Gorrin, S.P., Arbelo, C.D., Mora, J.L., 2002. Aggregates stability and water erosion in andosols of the canary islands. Land Degrad. Dev. 13, 515–523.
Schiettecatte, W., Gabriels, D., Cornelis, W.M., Hofman, G., 2008a. Enrichment of organic carbon in sediment transport by interrill and rill erosion processes. Soil Sci. Soc. Am. J. 72 (1), 50.
Schiettecatte, W., Verbist, K., Gabriels, D., 2008b. Assessment of detachment and sediment transport capacity of runoff by field experiments on a silt loam soil. Earth Surf. Proc. Land. 33 (8), 1302–1314.
Sharpely, A.N., Williams, J.R., 1990. EPIC, Erosion Productivity Impact Calculator: 1. Model Documentation. US Dept. Agric. Tech. Bull. No. 1768.
Shen, H., Zheng, F., Wen, L., Han, Y., Hu, W., 2016. Impacts of rainfall intensity and slope gradient on rill erosion processes at loessial hillslope. Soil Till. Res. 155, 429–436.
Shi, Z.H., Fang, N.F., Wu, F.Z., Wang, L., Yue, B.J., Wu, G.L., 2012. Soil erosion processes and sediment sorting associated with transport mechanisms on steep slopes. J. Hydrol. 454–455, 123–130.
Slattery, M.C., Bryan, R.B., 1992. Hydraulic conditions for rill incision under simulated rainfall: a laboratory experiment. Earth Surf. Proc. Land. 17 (2), 127–146.
Smith, P., Smith, J.U., Powlson, D.S., McGill, W.B., Arah, J.R.M., Chertov, O.G., Coleman, K., Franko, U., Frolking, S., Jenkinson, D.S., Jensen, L.S., Kelly, R.H., Klein-Gunnewiek, H., Komarov, A.S., Li, C., Molina, J.A.E., Mueller, T., Parton, W.J., Thornley, J.H.M., Whitmore, A.P., 1997. A comparison of the performance of nine soil organic matter models using datasets from seven long-term experiments. Geoderma 151, 152–225.
Starr, G.C., Lal, R., Malone, R., Hothem, D., Owens, L., Kimble, J., 2000. Modeling soil carbon transported by water erosion processed. Land Degrad. Dev. 11, 83–91.
Swanson, N.P., Dedrick, A.R., 1967. Soil particles and aggregates transported in water runoff under various slope conditions using simulated rainfall. Trans. ASAE 10 (2), 246–247.
Walkley, A., Black, I.A., 1934. An examination of the Degtjareff method for determining soil organic matter, and a proposed modification of the chromic acid titration method. Soil Sci. 37 (1), 29–38.
Wang, J., Zheng, F., Jiang, Z., Zhang, X., 2007. Assessment of WEPP model applicability (Hillslope Version) on Hill-gully Region of the Loess Plateau——a case study in slope length factor. Bull. Soil Water Conserv. 27 (2), 50–55 (In Chinese).
Wang, L., Shi, Z.H., 2015. Size selectivity of eroded sediment associated with soil texture on steep slopes. Soil Sci. Soc. Am. J. 79 (3), 917.
Wang, X., Cammeraat, E.L.H., Cerli, C., Kalbitz, K., 2014. Soil aggregation and the stabilization of organic carbon as affected by erosion and deposition. Soil Biol. Biochem. 72, 55–65.
Willmott, C.J., 1981. On the validation of models. Phys. Geogr. 2, 184–194.
Yitbarek, T.W., Belliethathan, S., Stringer, L.C., 2012. The onsite cost of gully erosion and cost-benefit of gully rehabilitation: a case study in Ethiopia. Land Degrad. Dev. 23, 157–166.
Zhang, G., Luo, R., Cao, Y., Shen, R., Zhang, X.C., 2010. Correction factor to dye-measured flow velocity under varying water and sediment discharges. J. Hydrol. 389 (1–2), 205–213.
Zhao, G., Mu, X., Wen, Z., Wang, F., Gao, P., 2013. Soil erosion, conservation, and eco-environment changes in the Loess Plateau of China. Land Degrad. Dev. 24, 499–510.
Zheng, F., 2006. Effect of vegetation changes on soil erosion on the Loess Plateau. Pedosphere 16 (4), 420–427.